SOCAR Proceedings

Injection & Producing Facilities

journal home page: http://proceedings.socar.az

EFFECT OF DEFORMATION ON PRECESSION DETAILS AT CRITICAL HEATING

A. G. Huseynov[1], F. S. Huseynli[1], Sh. A. Asadov*[1], N. M. Mirzezade[2]

[1]*Azerbaijan Technical University, Baku, Azerbaijan*

[2]*Azerbaijan National Aerospace Agency, Baku, Azerbaijan*

A B S T R A C T

The research work is devoted to a comprehensive analysis of thermal stresses and deformations arising on the working surface of prestressed components operating under critical temperature regimes. During service, these components are subjected to a combination of high temperatures, mechanical pressure, and frictional effects, which lead to complex thermo-mechanical interactions and non-uniform heat distribution across the contact surface. Such conditions significantly influence the stress–strain state, potentially causing structural instability, loss of functionality, or premature failure. To investigate these phenomena, mathematical models based on Fourier series expansions and governing differential equations of heat conduction and elasticity were developed. These models enable the determination of temperature fields, as well as the calculation of thermal stresses and displacements within both zero-order and first-order approximations. The analytical approach provides insight into the distribution patterns of stresses and allows the identification of critical zones where maximum thermal loading occurs. The practical significance of the study lies in the application of the obtained analytical results to engineering design. Based on the developed models, constructive and technological solutions are proposed to minimize the risk of critical stresses and excessive deformations on the working surface of prestressed parts. In addition, optimization of normal and contact stresses is carried out by defining permissible parameter ranges, taking into account the thermophysical and mechanical properties of the material, as well as surface quality indicators such as roughness and hardness. These findings contribute to improving the reliability, durability, and operational efficiency of prestressed components under severe thermal conditions.

Keywords: surface; deformation; precession part; critical heating; mathematical model.

Date submitted: 17.04.2026 **Date accepted:** 04.05.2026

© 2026 «OilGasScientificResearchProject» Institute. All rights reserved.

1. Introduction

The stress-strain state of the working surface of prestressed components under critical temperature conditions is examined. In this section, particular attention is paid to the thermal stress-strain behavior of the material when the temperature at the working surface reaches a critical value, denoted as T*. This critical temperature represents the threshold beyond which significant changes in the mechanical properties of the material may occur, including thermal softening, phase transformations, or the initiation of microstructural damage.

The analysis focuses on the behavior of the prestressed part's surface layer under these extreme thermal conditions. The stress-strain state is evaluated to determine the influence of elevated temperature on the internal distribution of thermal stresses, as well as on the stability and integrity of the component. Understanding the thermo-mechanical response at T∗T*T∗ is essential for predicting failure modes, ensuring the reliability of the prestressed structure, and designing components capable of withstanding transient thermal loads.

By characterizing the stress field at this critical point, it is possible to assess the degree of risk associated with thermal fatigue, thermal expansion mismatch, and stress concentration zones that may develop due to steep temperature gradients on the surface. This analysis forms a vital part of the overall thermal durability assessment of prestressed mechanical elements operating in high-temperature environments.

2. Main part

Let us now consider the problem of determining thermal stresses that develop on the inner surface of prestressed components under an overheated regime. In this regime, the temperature exceeds normal operational limits, resulting in intensified thermal gradients and elevated levels of thermoelastic stress within the material. The inner surface of prestressed parts, being in direct contact with high-temperature media or subjected to rapid thermal cycling, is particularly vulnerable to localized stress concentrations.

Under these conditions, the mismatch between thermal

**E-mail:* shamkhal.asadov@mail.ru

http://dx.doi.org/10.5510/OGP20260201204

expansion and the constraints imposed by prestressing leads to the generation of complex stress fields. These stresses may include both radial and tangential components, which must be evaluated accurately to predict potential structural degradation, such as crack initiation or propagation, plastic deformation, or even delamination in layered structures.

The analysis of the overheated regime requires solving the thermoelastic equations with boundary conditions reflecting the elevated and often non-uniform temperature distribution. It is especially important to consider temperature-dependent material properties, such as thermal conductivity, modulus of elasticity, and the coefficient of thermal expansion, as they significantly influence the stress response in this regime.

By quantifying the thermal stresses on the inner surface, engineers and researchers can assess the safety margins of prestressed components, optimize cooling or insulation strategies, and design against catastrophic thermal failure in high-temperature applications.

The thermo-stress state of prestressed components can be regarded as being in mechanical equilibrium under the action of body (volume) forces induced by the non-uniform temperature field that develops during operation [1, 2]. In practical scenarios, the operation of such components often leads to spatial temperature gradients due to external heating, internal friction, or interaction with high-temperature environments. These temperature gradients result in differential thermal expansion within the material, which in turn generates internal stresses even in the absence of external mechanical loading.

The equilibrium condition implies that the internal stress distribution compensates for these thermally induced body forces, ensuring the structural integrity of the component under steady or transient thermal loads. This state is governed by the equations of thermoelasticity, which couple the mechanical equilibrium equations with thermal conduction equations, taking into account temperature-dependent material properties and boundary conditions.

In prestressed systems, this interaction is further complicated by the initial stress field introduced during manufacturing or assembly (e.g., interference fits, thermal shrink fitting). Therefore, the total stress state must be evaluated as the superposition of the initial prestress and the additional thermal stresses arising from the operational temperature field (fig. 1).

A thorough understanding of this equilibrium condition is essential for accurately predicting the development of stress concentrations, assessing thermal fatigue life, and identifying potential failure mechanisms in prestressed components subjected to fluctuating thermal environments [4, 5].

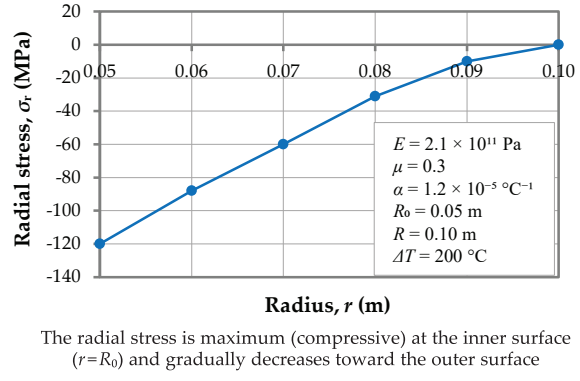

The radial stress is maximum (compressive) at the inner surface ($r=R_0$) and gradually decreases toward the outer surface

Fig. 1. Radial stress distribution along the thickness of the component

Without a precise grasp the interaction between thermally induced volume forces and the initial prestress states, it becomes challenging to model the true mechanical response of the material under service conditions. Such predictive capabilities are crucial not only for ensuring the structural reliability and long-term durability of components, but also for informing design decisions, material selection, and the implementation of thermal management strategies in high-performance engineering applications.

$$X = -\frac{\alpha E}{1-2\mu}\frac{\partial T}{\partial x}; \quad Y = -\frac{\alpha E}{1-2\mu}\frac{\partial T}{\partial y} \tag{1}$$

Here, α denotes the coefficient of linear thermal expansion, which quantifies the material's tendency to expand or contract in response to changes in temperature. For analytical convenience, the geometry of the inner contour of the component is assumed to be approximately circular, as indicated in expression (1). To simplify the mathematical formulation, a transition is made from the general polar coordinate system to one aligned with the geometry of the prestressed component.

In this adapted coordinate system, the origin of the concentric circles, denoted by (r, θ), is located at the geometric center of the inner surface. The inner and outer radii of the considered surface are denoted as R_0 and R, respectively. This allows for a more precise definition of the geometry for further analytical derivations.

To account for surface imperfections, certain cases of microroughness present on the inner surface of the cylindrical or pipe-like structures are also taken into consideration. These micro-irregularities can significantly affect local stress concentrations and the overall stress-strain response under thermal loading [6].

Let the boundary of the inner contour be denoted as L. We now introduce this boundary condition into expression (1) to incorporate the geometric and material parameters into the formulation of the thermal stress problem. This will enable a more accurate representation of the mechanical response of the prestressed part under non-uniform temperature distributions and realistic surface conditions.

The boundary conditions of the thermal stress problem on the inner surface of the pipe are defined in the following form:

$\sigma_n = -p(\theta)$; $\tau_{nt} = -fp(\theta)$ – in the contact area

$\sigma_n = 0$; $\tau_{nt} = 0$ – outside the contact area

$r = R_0$ – on the outer part of the pretension details:

$v_r = 0$; $v_\theta = 0$

The solution to the thermal voltage problem based on the superposition principle is presented as follows:

$$\sigma_r = \sigma_r^{(u)} + \sigma_r^{(T)}, \quad \sigma_\theta = \sigma_\theta^{(u)} + \sigma_\theta^{(T)}, \quad \tau_{r\theta} = \tau_{r\theta}^{(u)} + \tau_{r\theta}^{(T)} \tag{2}$$

here the first set $\sigma_r^{(u)}$; $\sigma_\theta^{(u)}$; $\tau_{r\theta}^{(u)}$, represents the solution of the isothermal elasticity theory problem for boundary conditions (1) – (2), the second set $\sigma_r^{(T)}$; $\sigma_\theta^{(T)}$; $\tau_{r\theta}^{(T)}$, represents the solution to the thermal stress problem in the absence of external forces and displacements at the internal boundary of the prestressed details:

$$r = \rho; \ \sigma_r^{(u)} = 0; \ \tau_{r\theta}^{(u)} = 0 \tag{3}$$

$$v_r^{(T)} = 0; \ v_\theta^{(T)} = 0; \ r = R_0 \tag{4}$$

(1) To solve the boundary problem for prestressed components, precise knowledge of the temperature distribution along the inner surface of these parts is essential. This is because the solution to a boundary problem fundamentally relies on accurately defining the thermal field, which directly influences the mechanical behavior of the material, the development of thermal stresses, and the overall thermoelastic response of the structure. In any structural element, particularly in prestressed components, non-uniform temperature distribution can lead to the formation of internal stresses and strains, potentially affecting the reliability and service life of the part [7-9]. Therefore, accurate determination of the temperature distribution is a prerequisite for correctly defining the boundary conditions. In this context, in the work of the authors [14], the required temperature distribution on the inner surface has already been determined either through analytical modeling or experimental measurements. This data now serves as the foundational input for advancing the mathematical and computational analysis of the boundary problem.

The boundary conditions are assumed as follows:

for the zeroth approximation –

$$v_r^{(0)} = 0;\ v_\theta^{(0)} = 0;\ r = R_0 \tag{5}$$

$$\sigma_r^{(0)} = 0;\ \tau_{r\theta}^{(0)} = 0;\ r = R_0 \tag{6}$$

for a first approximation –

$$\sigma_r^{(1)} = N;\ \tau_{r\theta}^{(1)} = T;\ r = R \tag{7}$$

$$v_r^{(1)} = 0;\ v_\theta^{(1)} = 0;\ r = R_0 \tag{8}$$

For convenience, the «T» index is not used in the stress and displacements, and the N and T functions are defined by formulas (2).

(2) The solution of the thermal stress problem involves addressing the case of a smooth boundary contour. In particular, when analyzing temperature-induced stresses in prestressed components, it is crucial to consider the geometry of the structure to simplify the formulation of the boundary conditions and ensure the applicability of the analytical methods. To obtain a solution for the thermal stress distribution in the wall section of the inner surface of prestressed parts (considered per unit height), the approach is based on the use of a thermal stress potential function related to displacement.

This approach allows for an iterative or approximated solution in which the potential function $\Phi(r,\theta)$ is determined for each approximation level. The function Φ represents the displacement potential under thermal loading and captures the effect of temperature gradients on the internal stress state of the material. The methodology follows the theoretical framework presented in [3], where detailed mathematical derivations and boundary condition formulations are provided. This approach enables an analytical description of the thermal stress field in a cylindrical or axisymmetric coordinate system, which is particularly relevant for hollow or ring-like prestressed structures [10-12].

In this problem, the displacement potential in the zeroth approximation is determined by the differential equation (1). The temperature function $t_0(r,\theta)$ is taken as a Fourier series (see formula 2). For the thermostress potential, the solution of equation (2) is assumed in the form (3). Substituting the functions (4) into the differential equation (3), $\Phi_n^{(0)}(r)(n=0,1,2,\ldots)$ we obtain a second-order inhomogeneous ordinary differential equation for the determination of the function (fig. 2):

$$\frac{d^2\Phi_n^{(0)}}{dr^2} + \frac{1}{r}\frac{d\Phi_n^{(0)}}{dr} - \frac{n^2}{r^2}\Phi_n^{(0)} = \frac{1+\mu}{1-\mu}\alpha F_n^{(0)} \tag{9}$$

We seek a particular solution of equation (9) by the method of variation of constants-

$$\Phi_0^{(0)} = \frac{1+\mu}{1-\mu}\alpha\left[-\ln r\int_R^r \rho F_0^{(0)}(\rho)d\rho + \int_r^{R_0}\rho F_0^{(0)}(\rho)\ln\rho d\rho\right], \tag{10}$$

$$\Phi_n^{(0)} = \frac{1+\mu}{1-\mu}\frac{\alpha}{2n}\left[r^n\int_r^{R_0}F_n^{(0)}(\rho)\rho^{-n}d\rho + r^{-n}\int_R^r F_n^{(0)}(\rho)\rho^n d\rho\right] \tag{11}$$

Similarly, $\Phi_n^{(0)}(r)(n=0,1,2,\ldots)$ an analogous solution is obtained for the function:

$$\Phi_n^{(0)} = \frac{1+\mu}{1-\mu}\frac{\alpha}{2n}\left[r^n\int_r^{R_0}B_n^{(0)}(\rho)\rho^{1-n}d\rho + r^{-n}\int_R^r B_n^{(0)}(\rho)\rho^{1+n}d\rho\right], \tag{12}$$

$$B_k^{(0)} = A_{10}^{(k)}r^k + A_{20}^{(k)}r^{-k}$$

Using formulas (2), (3) and relations (4), (5) in in the work of the authors [14] according to formula (6), the corresponding stresses $\sigma_r^{-(0)}\ \sigma_\theta^{-(0)};\ \tau_{r\theta}^{-(0)}$ and displacements $v_r^{-(0)}$ and $v_\theta^{-(0)}$ can be calculated.

The obtained stresses and displacements (not explicitly given here) do not satisfy the boundary conditions of the thermal stress state (7).

Therefore, a second stress-strain state is required.

$\overline{\sigma_r^{(0)}};\ \overline{\sigma_\theta^{(0)}};\ \overline{\tau_{r\theta}^{(0)}};\ \overline{v_r^{(0)}};\ \overline{v_\theta^{(0)}}$ is required to find —

$$\sigma_r^{(0)} = \sigma^-{}_r^{(0)} + \overline{\sigma_r^{(0)}} = 0, \tau_{r\theta}^{(0)} = \tau^-{}_{r\theta}^{(0)} + \overline{\tau_{r\theta}^{(0)}} = 0,\ r = R \tag{13}$$

$$v_r^{(0)} = \overline{v}_r^{(0)} + \overline{v_r^{(0)}} = 0, v_\theta^{(0)} = \overline{v}_\theta^{(0)} + \overline{v_\theta^{(0)}} = 0,\ r = R_0 \tag{14}$$

By solving the usual problem of elasticity theory, the following expression is obtained:

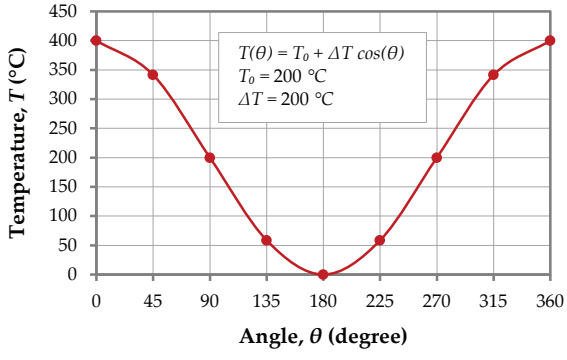

The temperature on the outer surface varies according to the cosine law, with maximum at θ=0° and minimum at θ=180°

Fig. 2. Temperature distribution along the inner surface

$$\overline{\overline{\sigma_r^{(0)}}} = \Gamma_2\left[a_0\alpha^2 - a_0'' - \left(a_0 - a_0\right)\frac{\alpha^2}{\rho^2}\right] + \left[\frac{\rho}{\alpha}a_1 + \Gamma_1\left(a_1 - b_1'\right)A + \Gamma_3\left(a_1 - a_1''\alpha\right)\Gamma\right]\cos\theta + \left[\frac{\rho}{\alpha}b_1 + \Gamma_1\left(b_1 + a_1'\right)A + \Gamma_3\Gamma\left(b_1 - b_1''\alpha\right)\right]\sin\theta + \sum_{k=2}^{\infty}\left[\left(\beta_k a_k + D_k a_k'' + \gamma_k b_k' + D_k' b_k''\right)\cos\theta + \left(\beta_k b_k + D_k b_k'' - \gamma_k a_k' - D_k' a_k''\right)\sin k\theta\right] \quad (15)$$

$$\overline{\overline{\sigma_\theta^{(0)}}} = \Gamma_2\left[a_0\alpha^2 - a_0'' + \left(a_0 - a_0''\right)\frac{\alpha^2}{\rho^2}\right] + \ldots + \sum_{k=2}^{\infty}\left[\left(\beta_k\alpha_k + D_k\dot{\alpha}_k + \gamma_k\dot{b}_k + \dot{D}_k\dot{b}_k\right)\cos\theta + \left(\beta_k b_k + D_k\dot{b}_k - \gamma_k a_k - \dot{D}_k\dot{a}_k\right)\sin k\theta\right] \quad (16)$$

$$\overline{\overline{\sigma_\theta^{(0)}}} = \Gamma_2\left[a_0\alpha^2 - a_0'' + \left(a_0 - a_0''\right)\frac{\alpha^2}{\rho^2}\right] + \left[3\frac{\rho}{\alpha}a_1 + \Gamma_1\left(a_1 - b_1'\right)\Gamma_4 + \Gamma_3\left(a_1 - a_1''\alpha\right)\Gamma_5\right]\cos\theta + \left[3\frac{\rho}{\alpha}b_1 + \Gamma_1\left(b_1 + a_1'\right)\Gamma_4 + \Gamma_3\left(b_1 - b_1''\alpha\right)\Gamma_5\right]\sin\theta + \sum_{k=2}^{\infty}\left[\left(\beta_k' a_k + M_k a_k'' + \gamma_k' b_1 + M_k' b_k''\right)\cos\theta + \left(\beta_k' b_k + M_k b_k'' - \gamma_k' a_k - M_k' a_k''\right)\sin k\theta\right] \quad (17)$$

$$\overline{\overline{\tau_{r0}^{(0)}}} = \frac{\dot{a}_0\alpha^2}{\rho^2} + \left[\frac{\rho}{\alpha}a_1 + \Gamma_1\left(a_1 - \dot{b}_1\right)\left(\Gamma_4 + 2\rho\right) + \Gamma_3\left(a_1 - a_1''\alpha\right)\Gamma\right]\sin\theta - \left[\frac{\rho}{\alpha}b_1 + \Gamma_1\left(b_1 + a_1'\right)\left(\Gamma_4 + 2\rho\right) + \Gamma_3\left(b_1 - b_1''\alpha\right)\Gamma\right]\cos\theta + \sum_{k=2}^{\infty}\left[\left(\gamma_k'' a_k + \Pi_k' a_k - \beta_k'' b_k - \Pi_k b_k''\right)\cos k\theta + \left(\beta_k a_k + \Pi_k a_k'' + \gamma_k'' b_k + \Pi_k' b_k\right)\sin k\theta\right] \quad (18)$$

here,

$$\gamma_k = \frac{1}{2K}\left\{\left(k-1\right)\left(k+2\right) - k^2\alpha^2 - \left(k-2\right)\alpha^{2k}\left(\frac{\rho}{\alpha}\right)^{k-2} + \left(k-2\right)\left(k+1\right) - k^2\alpha^2 + \left(k+2\right)\alpha^{2k}\left(\frac{\rho}{\alpha}\right)^{k+2} + k\left(k+1\right) - k\left(k+2\right)\alpha^2 + k\alpha^{2k}\left(\frac{\rho}{\alpha}\right)^{k} + k\left(k-1\right) - k\left(k-2\right)\alpha^2 - k\alpha^{2k}\left(\frac{\rho}{\alpha}\right)^{k}\right\} \quad (19)$$

$$a_k = -G\beta R_0^{k-2}\left(R_0 + k\right)\int_R^{R_g} F_R^{(0)}\left(\rho\right)\rho^{1+k}d\rho, \ \left(k = 0,1,2,\ldots\right) \quad (20)$$

$$b_k = G\beta R_0^{k-2}\left(R_0 + k\right)\int_R^{R_g} B_R^{(0)}\left(\rho\right)\rho^{1+k}d\rho, \quad \left(k = 1,2,\ldots\right) \quad (21)$$

$$a_k = G\beta R_0^{k-2}\left(1 + k\right)\int_R^{R_g} B_R^{(0)}\left(\rho\right)\rho^{1+k}d\rho, \quad \left(k = 0,1,2,\ldots\right) \quad (22)$$

$$b_k'' = -G\beta R_0^{k-2}\left(1 + k\right)\int_R^{R_0} F_k^{(0)}\left(\rho\right)\rho^{1+k}d\rho, \quad \left(k = 1,2,\ldots\right) \quad (23)$$

$$a_k = G\beta R^{k-2}\left(R - k\right)\int_R^{R_0} F_R^{(0)}\left(\rho\right)\rho^{1-k}d\rho, \quad \left(k = 0,1,2,\ldots\right) \quad (24)$$

$$b_k = G\beta R^{k-2}\left(R - k\right)\int_R^{R_0} B_R^{(0)}\left(\rho\right)\rho^{1-k}d\rho, \quad \left(k = 1,2,\ldots\right) \quad (25)$$

$$a_k = G\beta R^{k-2}\left(1 - k\right)\int_R^{R_0} B_R^{(0)}\left(\rho\right)\rho^{1-k}d\rho, \quad \left(k = 0,1,2,\ldots\right) \quad (26)$$

$$b_k = -G\beta R^{k-2}\left(1 - k\right)\int_R^{R_0} F_R^{(0)}\left(\rho\right)\rho^{1-k}d\rho, \quad \left(k = 1,2,\ldots\right) \quad (27)$$

$$\beta = \frac{1+\mu}{1-\mu}\alpha$$

$$\sigma_r^{(0)} = \overline{\sigma}_r^{(0)} + \overline{\overline{\sigma_r^{(0)}}}, \ \ \sigma_\theta^{(0)} = \overline{\sigma}_\theta^{(0)} + \overline{\overline{\sigma_\theta^{(0)}}}, \ \ \tau_{r\theta}^{(0)} = \overline{\tau}_{r\theta}^{(0)} + \overline{\overline{\tau_{r\theta}^{(0)}}} \quad (28)$$

The temperature stresses in the zero approximation of prestressed details are determined using the formulas.

In the first approximation, the thermoelastic displacement potential is determined by solving the differential equation (28). The temperature function $t^{(1)}(r,\theta)$ is taken as a Fourier series (see formula 16). The solution of equation (14) for the thermoelastic potential is given in the form (15). The functions $\Phi_n^{(1)}(r)$ and $\Phi_n^{*(1)}(r)$ are determined as:

$$\Phi_0^{(1)} = \frac{1+\mu}{1-\mu}\alpha \times \times\left[-\ln r\int_r^{R_0} F_0^{(1)}\left(\rho\right)\rho d\rho + \int_r^{R_0}\rho F_0^{(1)}\left(\rho\right)\ln\rho d\rho\right] \quad (29)$$

$$\Phi_n^{(1)} = -\frac{1+\mu}{1-\mu}\frac{\alpha}{2n}\times \times\left[r^n\int_r^{R_0} F_n^{(1)}\left(\rho\right)\rho^{1-n}d\rho + r^{-n}\int_R^{r} F_n^{(1)}\left(\rho\right)\rho^{1+n}d\rho\right] \quad (30)$$

$$\Phi_n^{(1)} = \frac{1+\mu}{1-\mu}\frac{\alpha}{2n}\times \times\left[r^n\int_r^{R_0} B_n^{(1)}\left(\rho\right)\rho^{1-n}d\rho + r^{-n}\int_R^{r} B_n^{(1)}\left(\rho\right)\rho^{1+n}d\rho\right] \quad (31)$$

$$F_k^{(1)} = C_{11}^{(k)}r^k + C_{21}^{(k)}r^{-k}, B_k^{(1)} = A_{11}^{(k)}r^k + A_{21}^{(k)}r^{-k}, F_0^{(1)} = C_{11} + C_{21}\ln r$$

By repeating the process of solving the problem, we first find $\overline{\sigma}_r^{(1)}$, $\overline{\sigma}_\theta^{(1)}$, $\overline{\tau}_{r\theta}^{(1)}$ the stresses and displacements $\overline{v}_r^{(1)}$, $\overline{v}_\theta^{(1)}$. Then, for this approximation, we find the second $\overline{\overline{\sigma_r^{(1)}}}$, $\overline{\overline{\sigma_\theta^{(1)}}}$, $\overline{\overline{\tau_{r\theta}^{(1)}}}$ stress-strain state and displacements $\overline{\overline{v_r^{(1)}}}$, $\overline{\overline{v_\theta^{(1)}}}$, according to the boundary conditions:

$$\overline{\overline{\sigma_r^{(1)}}} = N - \overline{\sigma}_r^{(1)}, \quad \overline{\overline{\tau_{r\theta}^{(1)}}} = T - \vec{\tau}_{r\theta}^{(1)} \quad \text{same as } r = R$$
$$\overline{\overline{v_r^{(1)}}} = -v_r^{(1)}, \quad \overline{\overline{v_\theta^{(1)}}} = -\overline{v}_r^{(1)} \quad \text{same as } r = R$$

By solving the boundary condition problem (7, 8) using the method explained earlier, the temperature stresses and displacements are determined to the first approximation.

$$\sigma_r^{(1)} = \overline{\sigma}_r + \overline{\overline{\sigma_r}}$$
$$\sigma_\theta^{(1)} = \overline{\sigma}_\theta + \overline{\overline{\sigma_\theta}}$$
$$v_r^{(1)} = \overline{v}_r + \overline{\overline{v_r}}$$
$$\tau_\theta^{(1)} = \overline{\tau}_{r\theta} + \overline{\overline{\tau_{r\theta}}}$$
$$v_\theta^{(1)} = \overline{v}_\theta + \overline{\overline{v_\theta}}$$

Here,

$$\overline{\overline{\sigma_r^{(1)}}} = \Omega_r^{(1)}; \ \ \overline{\overline{\sigma_\theta^{(1)}}} = \Omega_\theta^{(1)}; \ \ \overline{\overline{\tau_{r\theta}^{(1)}}} = \Omega_{r0}^{(1)} \quad (32)$$

$\Omega_r^{(1)}$, $\Omega_\theta^{(1)}$, and $\Omega_{r\theta}^{(1)}$ the quantities form the right-hand

sides of formulas (32), respectively, and it should be assumed here that.

$$a_k = -G\beta I R_0^{-k-2}\left(R_0 + k\right), \quad \left(k = 0,1,2,\ldots\right) \tag{33}$$
$$b_k = -G\beta I_1^{(1)} R_0^{-k-2}\left(R_0 + k\right), \quad \left(k = 0,1,2,\ldots\right)$$
$$\dot{a}_k = -G\beta I_1^{(1)} R_0^{-k-2}\left(1 + k\right), \quad \left(k = 0,1,2,\ldots\right)$$
$$\dot{b}_k = -G\beta I^{(1)} R_0^{-k-1}\left(1 + k\right), \quad \left(k = 0,1,2,\ldots\right)$$
$$\ddot{a}_k = -G\beta I_2^{(1)} R^{-k-2}\left(R - k\right), \quad \left(k = 0,1,2,\ldots\right)$$
$$\ddot{b}_k = G\beta I_3^{(1)} R^{-k-2}\left(R - k\right), \quad \left(k = 0,1,2,\ldots\right)$$
$$\dddot{a}_k = -G\beta I_3^{(1)} R^{k-2}\left(1 - k\right), \quad \left(k = 0,1,2,\ldots\right)$$
$$\dddot{b}_k = -G\beta I_2^{(1)} R^{k-2}\left(1 - k\right), \quad \left(k = 0,1,2,\ldots\right) \tag{34}$$

The presented method allows to determine the temperature stresses in the part during the operation of prestressed parts in the critical thermal state (fig. 3). The total stress components are determined by formulas (34).

For the purpose of strength assessment for prestressed details, the normal and shear stress $r=\rho(\theta)$ are defined (table).

$$\sigma_* = \sigma_{0|r=R}^{(0)} + \frac{\partial \sigma_0^{(0)}}{\partial_r} \varepsilon H\left(\theta\right) + \varepsilon \sigma_0^{(1)} \tag{34}$$

This is a polar angle. Θ is a function. If the following robustness condition is satisfied:

$$\sigma_{max} = \sigma_0$$

and if σ_0 is the yield strength of the material of the prestressed parts, then permanent deformations will occur. If σ_0 the brittle strength of the material is, the fulfillment of conditions (7, 8) means a violation of the integrity of the pipe material (the formation of surface cracks). During the process, these cracks gradually spread into the depth of the material [13-15]. Although they are very thin, they cause the concentration of large stresses. The calculations show that due to high temperature on the inner surface of the prestressed parts, thermal stresses arise that exceed the stresses arising from force loads on the working surface. Therefore, at the production and design stages, the following conditions must be met through constructive and technological solutions

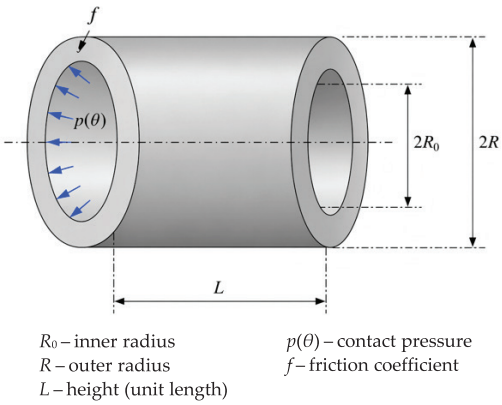

Fig. 3. Geometry of the prestressed cylindrical component

Table

Calculated stress values

Radius, r (m)	Radial stress, σ_r (MPa)	Tangential stress, σ_θ (MPa)	Shear stress, $\tau_{r\theta}$ (MPa)
0.050 (=R_0)	–120.0	–85.4	0.0
0.060	–90.3	–63.7	–5.1
0.070	–60.2	–40.8	–7.6
0.080	–35.6	–22.5	–6.2
0.090	–15.8	–9.6	–2.6
0.100 (=R_0)	0.0	0.0	–2.66

Note: Negative sign indicates compressive stress

$$T = T_*, \quad \sigma_{max} = \sigma_0$$

As a result, compensation of the inequality allows us to determine the ranges of permissible values of the parameters of the contact pair details.

Conclusion

As a result of the conducted research, it was determined that thermal stresses and associated deformations developing on the inner surface of prestressed components under critical temperature conditions exert a significant influence on the operational reliability and structural integrity of these parts. The findings obtained through comprehensive analytical and mathematical modeling revealed that non-uniform temperature distributions on the inner surface lead to the formation of localized thermal stress concentrations.

These stresses, induced solely by thermal gradients, were shown to exceed the levels typically generated by mechanical loading alone. Under high-temperature exposure, the material experiences increased internal energy, which in turn causes localized yielding, thermal softening, and in some cases, embrittlement of the surface layer. Once the thermal stresses surpass the yield strength or approach the brittleness threshold of the material, permanent plastic deformations occur and surface-initiated cracks begin to develop.

This degradation process poses a critical threat to the performance and service life of the component, particularly in high-temperature or cyclic thermal environments. Therefore, understanding the thermoelastic behavior and identifying the thresholds for critical stress states are essential for the design and safe operation of prestressed structures subjected to elevated thermal loads.

The study demonstrated that under critical temperature conditions, hazardous thermal stresses develop on the inner surface of prestressed components, which may ultimately lead to a compromise in their structural strength and reliability. These thermally induced stresses, often exceeding the material's elastic limit, contribute to the initiation of failure mechanisms such as plastic deformation, microcracking, and delamination, particularly in regions with stress concentrations or geometric discontinuities.

Therefore, it becomes imperative that during the design and manufacturing stages of prestressed parts, particular attention must be given to ensuring an optimal distribution of both thermal and mechanical loads. This can be achieved through a combination of constructive design strategies, such as geometrical optimization and the inclusion of thermal compensation features, and technological measures, including controlled heat treatment, surface strengthening techniques, and material selection based on thermal compatibility.

The mathematical models and analytical approaches proposed in this study, formulated based on realistic boundary conditions, offer a reliable framework for the precise evaluation of both normal and contact stresses at the critical contact interfaces. By employing these methods, engineers can define allowable stress limits with higher accuracy and ensure safe operation of components within their thermal and mechanical capacity under service conditions.

Consequently, to mitigate the adverse effects of critical temperature regimes on the inner surface of prestressed components, it is essential to implement the following measures:

- Optimization of material selection by ensuring that the thermophysical and mechanical properties are well-suited to the operational conditions and loading requirements;
- Improvement of surface technological processing to increase dimensional accuracy and minimize microdefects that may act as stress concentrators;
- Effective management of thermal regimes, including the application of advanced cooling systems to control temperature gradients and reduce thermal fatigue;
- Implementation of constructive design solutions aimed at reducing stress concentrations and distributing internal tensions more uniformly.

This study contributes to advancing the reliability, service life, and technical safety indicators of prestressed components. By integrating these measures into the design and manufacturing process, the research supports the development of more durable and resilient next-generation products capable of operating under severe thermal and mechanical environments.

References

1. Huseynov, A. G., Huseynli, F. S., Huseynzade, M. B. (2026). Analytical calculation of contact pressure under thermoelastic deformation conditions in sucker rod pumps. *SOCAR Proceedings*, 1, 99-108.

2. Abbasov, V., Amirov, F., Karimov, A. (2025). Wear properties of camshaft cams and improvement of their wear resistance. Reliability: *Theory & Applications*, 20(SI7(83)), 297–303.

3. Bashirov, R. J., Rasulov, F. R. (2022). Formation of high strength and corrosion resistance composition cover on the surface of casting. *Kazakhstan: Eurasian Journal of Physics and Functional Materials*, 6(4), 285-297.

4. Gilaev, G. G., Khabibullin, M. Ya., Bakhtizin, R. N. (2023). Improvement of methods for combat with sand in production wells. *SOCAR Proceedings*, 1, 87–93.

5. Guliev, H. F., Seyfullaeva, Kh., I. (2022). Optimal control problem with coefficients for the equation of vibrations of a thin plate with discontinuous solution. *Proceedings of the Institute of Mathematics and Mechanics of Azerbaijan. Academy of Sciences*, 48(2), 238–248.

6. Huseynov, A., Huseynli, F., Safarov, M. (2025). Reliability prediction of precision parts of fuel pumps with enhanced surface hardness achieved through laser technology. *Tribologia – Finnish Journal of Tribology*, 42(1–2), 64–71.

7. Huseynov, A. G., Nazarov, I. A, Huseynli, F. S., Safarov, M. (2025, May). Determinatıon of deformation and machining allowance of precision parts hardened by laser method. *Reliability: Theory & Applications*, 7 (83), 20, 379–385.

8. Huseynov, A., Nazarov, I., Huseynli, F., Safarov, M. (2025). Challenges of property inheritance during the technological processing of fuel pump precision parts. *Tribologia - Finnish Journal of Tribology*, 42(1–2), 72–79.

9. Jamalbayov, M. A., Valiyev, N. A., Ibrahimov, Kh. M., et al. (2024). Energy and efficiency optimization in sucker-rod pumping using discrete-imitation modeling concept: Application to well operations in the Bibi-Heybat field of Azerbaijan. *SOCAR Proceedings*, SI1, 95–101.

10. Karimov, A. F. (2024, May). Improvement of the design and production of camshafts. In book: «Innovative equipment and technologies in mechanical engineering» Vol. 17. *St. Petersburg: Research Center MS.*

11. Mohanty, R. R., Girina, O. A., Fonstein, N. M. (2011). Effect of heating rate on the austenite formation in low-carbon high-strength steels annealed in the intercritical region. *Metallurgical and Materials Transactions A*, 42, 3680–3690.

12. Bashirov, R. J., Veysov, R. A., Astanova, E. R., et al. (2025). Restoration technologies for precision diesel injector components using vacuum chromotitanizing and grinding. *SOCAR Proceedings*, 3, 164-169.

13. Rasulov, F. R. (2020). Mathematical model of crystallization and cooling process of coated casting. In: *The 7th International Conference on Control and Optimization With İndustrial Applications, Baku, 26–28 August.*

14. Sun, X., Li, Y. (2019). Comparison of hot deformation behaviour and microstructural evolution between PM and IM alloys. *Materials & Design*, 165, 107582.

15. Tang, G., Zhang, J. (2024). Temperature–strain prediction driven by deformation induced heating in SCM440 steel. *Heliyon*, 10(4), e26322.

16. Abdullayev, V. M. (2018). Numerical solution to optimal control problems with multipoint and integral conditions. *Proceedings of the Institute of Mathematics and Mechanics of Azerbaijan. Academy of Sciences*, 44(2), 171–186.

17. Wang, X. (2022). Effect of residual deformation energy and critical heating rate on cubic texture and grain growth behavior of severely deformed aluminum foil. *Materials*, 15(4), 1395.

18. Wu, M., Liu, W., Xiao, D., et al. (2023). Influence of thermal exposure on the microstructure and mechanical behaviors of an Al–Cu–Li alloy. *Materials & Design*, 241, 111767.

19. Yan, H., Wang, W., Zhang, S., Ma, S. (2022). Microstructure and thermal deformation behavior of hot pressing sintered Zr–6Al–0.1B alloy. *Materials*, 15(5), 1816.

20. Zhao, J., Wang, J., Li, J. (2024). The effects of super-fast heating rate and holding time on the microstructure and properties of DP Fe-0.16C-1.4Mn sheet steel. *Materials*, 17(20), 4982.